Influence of the source's energy fluctuation on computational ghost imaging and effective correction approaches

Xiaodong Mei (梅笑冬)[1,2], Chenglong Wang (王成龙)[1], Yami Fang (方亚秒)[3], Ting Song (宋 婷)[3], Wenlin Gong (龚文林)[1,*], and Shensheng Han (韩申生)[1]

[1]*Key Laboratory for Quantum Optics and Center for Cold Atom Physics of CAS, Shanghai Institute of Optics and Fine Mechanics, Chinese Academy of Sciences, Shanghai 201800, China*

[2]*University of Chinese Academy of Sciences, Beijing 100049, China*

[3]*Shanghai Key Laboratory of Aerospace Intelligent Control Technology, Shanghai Aerospace Control Technology Institute, Shanghai 201800, China*

**Corresponding author: gongwl@siom.ac.cn*

Received September 18, 2019; accepted December 26, 2019; posted online April 14, 2020

We investigate the influence of the source's energy fluctuation on both computational ghost imaging and computational ghost imaging via sparsity constraint, and if the reconstruction quality will decrease with the increase of the source's energy fluctuation. In order to overcome the problem of image degradation, a correction approach against the source's energy fluctuation is proposed by recording the source's fluctuation with a monitor before modulation and correcting the echo signal or the intensity of computed reference light field with the data recorded by the monitor. Both the numerical simulation and experimental results demonstrate that computational ghost imaging via sparsity constraint can be enhanced by correcting the echo signal or the intensity of computed reference light field, while only correcting the echo signal is valid for computational ghost imaging.

Keywords: ghost imaging; speckle; image reconstruction.
doi: 10.3788/COL202018.042602.

Computational ghost imaging (CGI) can image an unknown target with only a single-pixel detector where the intensity distribution of the reference light field is computed or prebuilt[1–6]. Up until now, there have been two types of typical implementation approaches for CGI. One is that some precise digital phase modulator, like a spatial light modulator (SLM), is utilized and the intensity distribution of the reference light field is obtained by a computation of the propagating field[2]. The other is that the intensity distribution of the reference light field is calibrated in advance[3,4]. Compared with traditional ghost imaging (TGI) with two arms, CGI has an obvious advantage in real-time imaging because only the modulation speed restricts the imaging speed. Later, when compressive sensing theory was introduced to the image reconstruction of CGI, sparsity of the target was taken as a prior constraint in reconstruction, and computational ghost imaging via sparsity constraint (CGISC) could obtain a high resolution image with the measurements below the Nyquist limit. This makes it possible to further improve the imaging speed of CGI due to less measurements required for image reconstruction[7]. This technique has aroused increasing interest in remote sensing[8], imaging through scattering media[9–11], and 3D computational imaging[12–14] in the most recent ten years.

However, for CGI, in order to guarantee a good imaging quality, some common orthogonal coding, like the Hadamard matrix and orthogonal Gauss matrix, is usually adopted for modulation of the light field[15–17]. The source's energy should be stable enough during the whole sampling process, which is the key point of CGI[16,17]. If the source's energy is unstable, the energy fluctuation is equivalent to a random multiplicative noise, which will lead to the rapid degradation of CGI, especially when the coding of the speckle pattern is orthogonal because the case is very sensitive to noise[18]. Unfortunately, in the application of remote sensing, due to a long detection distance, a single pulsed energy of the laser used in the CGI system is very high and sometimes its energy fluctuation can reach 10%. Therefore, some approaches against the source's energy fluctuation should be considered for CGI, especially for applications like remote sensing and super-resolution imaging. In this Letter, we first analyze the influence of the source's energy fluctuation on both CGI and CGISC. Then, two correction approaches against the source's energy fluctuation are proposed based on correcting the echo signal or the intensity of the computed reference light field. Later, the approaches' validity is demonstrated by both numerical simulation and experiments. Finally, we apply the approach of correcting the echo signal to our CGI lidar system and successfully enhance the reconstruction quality.

For CGI, as shown in Fig. 1(a), a laser beam passes through a modulator and then illuminates the object. The photons transmitted through the object are collected by a bucket detector. In the framework of CGI,

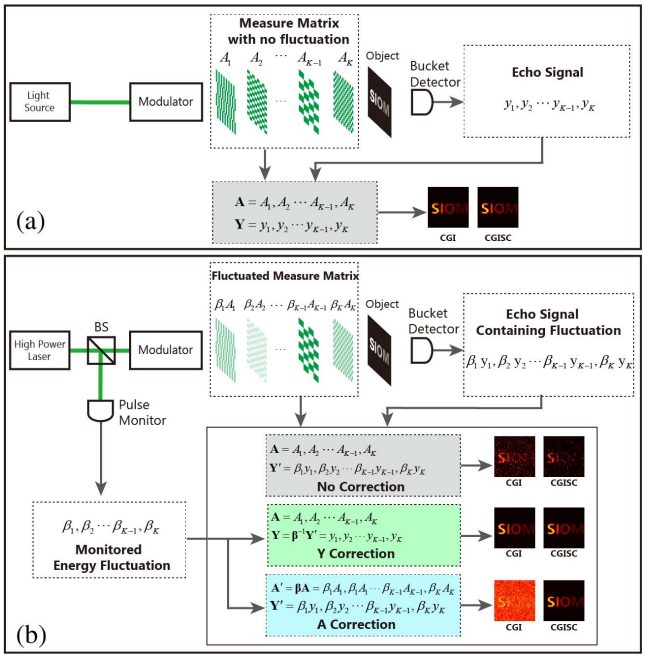

Fig. 1. Schematics of the (a) standard CGI and (b) CGI with A or Y Correction.

the object's image $\mathbf{O}_{\mathrm{CGI}}$ can be reconstructed by computing the coded speckle patterns $\mathbf{A}$ and the echo signal $\mathbf{Y}$ recorded by the bucket detector[19],

$$\mathbf{O}_{\mathrm{CGI}} = (\mathbf{A} - \mathbf{I}\langle\mathbf{A}\rangle)^T\mathbf{Y}, \tag{1}$$

where $\mathbf{A}$ is a $K \times N$ matrix, K is the total measurement number, and N is the reshaped size of the object. $\mathbf{I}$ is a $K \times 1$ column vector whose elements are all 1, $\mathbf{Y}$ is a $K \times 1$ column vector, and $\mathbf{Y} = \mathbf{AX}$. $\mathbf{X}$ is an $N \times 1$ column vector and denotes the object's transmission function.

For CGISC, the object's image can be reconstructed by solving the convex optimization[8]

$$\mathbf{O}_{\mathrm{CGISC}} = \arg\min\frac{1}{2}\|\mathbf{Y} - \mathbf{AX}\|_2^2 + \tau\|\alpha\|_1, \tag{2}$$

where τ is a nonnegative parameter, and $\|V\|_1$ and $\|V\|_2$ respectively denote the ℓ_1-norm and the Euclidean norm of V. In addition, α is the sparse representation of $\mathbf{X}$ on a given representation basis (namely, $\mathbf{X} = \mathbf{\Psi}\alpha$ and $\mathbf{\Psi}$ denotes the transform operator to the sparse representation basis).

As shown in Fig. 1(b), when the pulsed laser's peak energy is unstable, the coded speckle patterns illuminating on the object will become $\mathbf{A}'$ instead of $\mathbf{A}$. In other words, each row of matrix $\mathbf{A}$ is multiplied by a random constant, namely

$$\mathbf{A}' = \mathbf{\beta A} = \begin{bmatrix} \beta_1 & 0 & \cdots & 0 \\ 0 & \beta_2 & & 0 \\ \vdots & & & \vdots \\ 0 & 0 & \cdots & \beta_K \end{bmatrix}\mathbf{A}, \tag{3}$$

where $\mathbf{\beta}$ is a $K \times K$ diagonal matrix, and β_i, $i = 1, 2, \ldots, K$ denote some nonnegative parameters that express the peak value of each pulse. Therefore, the pulsed laser's energy fluctuation will lead to the intensity fluctuation of the echo signal $\mathbf{Y}$, which makes $\mathbf{Y}$ become $\mathbf{Y}' = \mathbf{\beta Y}$ and means that there is a random multiplicative noise for the detection process ($\mathbf{Y}' \neq \mathbf{AX}$). In this case, if we exploit the matrices $\mathbf{A}$ and $\mathbf{Y}'$ [namely, the data of "No Correction" displayed in Fig. 1(b)] for reconstruction in CGI and CGISC, the imaging results will decay with the increase of the source's energy fluctuation. In order to overcome the influence of the source's energy fluctuation on CGI and CGISC, as displayed in Fig. 1(b), a small part of the energy emitted from the laser is divided by a beam splitter (BS) and is detected by a monitor like a PIN diode before modulation, which can record the peak value of each pulse (namely, the diagonal matrix $\mathbf{\beta}$ can be achieved). We have proposed two methods by correcting $\mathbf{A}$ or $\mathbf{Y}'$, which makes the detection process satisfy $\mathbf{Y} = \mathbf{AX}$ or $\mathbf{Y}' = \mathbf{A}'\mathbf{X}$.

(1) Y Correction: as shown in the green block in Fig. 1(b), $\mathbf{Y}$ is obtained by $\mathbf{Y} = \mathbf{\beta}^{-1}\mathbf{Y}'$; CGI and CGISC by using the data $\mathbf{A}$ and $\mathbf{Y}$.

(2) A Correction: as shown in the blue block in Fig. 1(b), $\mathbf{A}'$ is obtained by $\mathbf{A}' = \mathbf{\beta A}$; CGI and CGISC by using the data $\mathbf{A}'$ and $\mathbf{Y}'$.

Furthermore, according to Ref. [20], the degree of laser energy fluctuation can be expressed by the root mean square (RMS), namely

$$\mathrm{RMS} = \frac{\sigma}{\mu}, \tag{4}$$

where σ is the standard deviation of the diagonal elements of matrix $\mathbf{\beta}$ and μ is the mean value of the diagonal elements of matrix $\mathbf{\beta}$.

In order to verify the validity of the proposed correction approach, numerical simulation and experiments are performed. The proof-of-principle experimental setup is shown in Fig. 2.

A 532 nm solid-state pulsed laser is controlled by a field programmable gate array (FPGA) to produce a light source with different energy fluctuations. The light source is divided into two paths by a beam splitter. In the

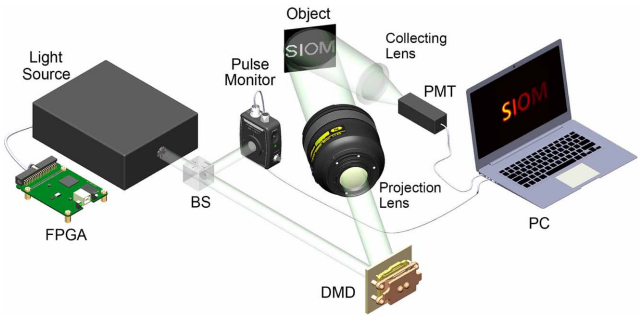

Fig. 2. Proof-of-principle experimental setup of the CGI with A or Y Correction for an unstable source.

reflection path, the laser beam is detected by a photodetector (pulse monitor) that is used to monitor the energy fluctuation of the pulsed laser. In the transmission path, the laser beam illuminates a digital micro-mirror device (DMD) and is modulated by the DMD, and then the reflection light is imaged onto the object by a 2.6× magnification projection lens. The object consists of four letters "SIOM" (30 mm × 30 mm) printed on an A4 paper and the gray intensity ratio of four letters is 1:0.8:0.6:0.4. Then the photons reflected from the object are converged onto a photomultiplier tube (PMT) by a collecting lens. The output signals of the pulse monitor and PMT are sampled by a high speed (2 GSa/s) analog-to-digital (ADC) board in the PC. The FPGA controlling the light source also synchronizes the DMD and ADC board. In addition, matrix **A** is a 4096 × 4096 Hadamard matrix corresponding to 64 × 64 pattern resolution and a 4096 sample number. Due to the limited pixel size of the DMD, we binned a 4 × 4 DMD pixel as one pattern pixel, so the transverse size of the coded speckle patterns at the DMD plane is 3.5 mm × 3.5 mm, corresponding to 256 × 256 DMD pixels. The numerical simulation parameters are the same as the experiment parameters.

Figures 3(I) and 3(II) present the numerical simulation and experimental results when the RMS of the laser's energy fluctuation is 0%, 2%, 4%, 6%, 8%, and 10%, respectively. From Figs. 3(I) and 3(II), it is clearly seen that the reconstruction quality of both CGI and CGISC will decrease as the increase of source's energy fluctuation. When the method of Y Correction or A Correction is exploited, CGISC can be obviously enhanced whereas only the method of Y Correction is valid for CGI.

To quantitatively measure the reconstruction quality of both CGI and CGISC, the reconstruction fidelity is estimated by calculating the structural similarity index (SSIM)[21],

$$\mathrm{SSIM}(x,y)=\frac{4\mu_x\mu_y\sigma_{xy}}{(\mu_x^2+\mu_y^2)(\sigma_x^2+\sigma_x^2)}, \tag{5}$$

where μ_x, μ_y are the average of the original image x and the reconstructed image y. σ_x and σ_y are the variance of x and y, and σ_{xy} is the covariance of x and y. In addition, the value of SSIM is 0–1, and the higher the value SSIM is, the more similar they are.

The dependence of SSIM on the RMS of the laser's energy fluctuation for different correction methods is illustrated in Fig. 4. Figure 4(a) is the SSIM-RMS curves of simulated results and Fig. 4(b) is the SSIM-RMS curves of experimental results. It is obviously observed that the experimental SSIM-RMS curves are consistent with the simulated results. For CGI, the reason of the invalidity of the A Correction method can be explained by the characteristic matrix $\mathbf{M_C}=(\mathbf{A}-\mathbf{I}\langle\mathbf{A}\rangle)^T\mathbf{A}$ described in Ref. [15]. From Eq. (1), when $\mathbf{M_C}$ is a scalar matrix, the object's image can be exactly reconstructed. Therefore, if $\mathbf{M_C}$ gets closer to a scalar matrix, then the reconstruction quality gets better. Figure 5 displays the diagrams of $\mathbf{M_C}$

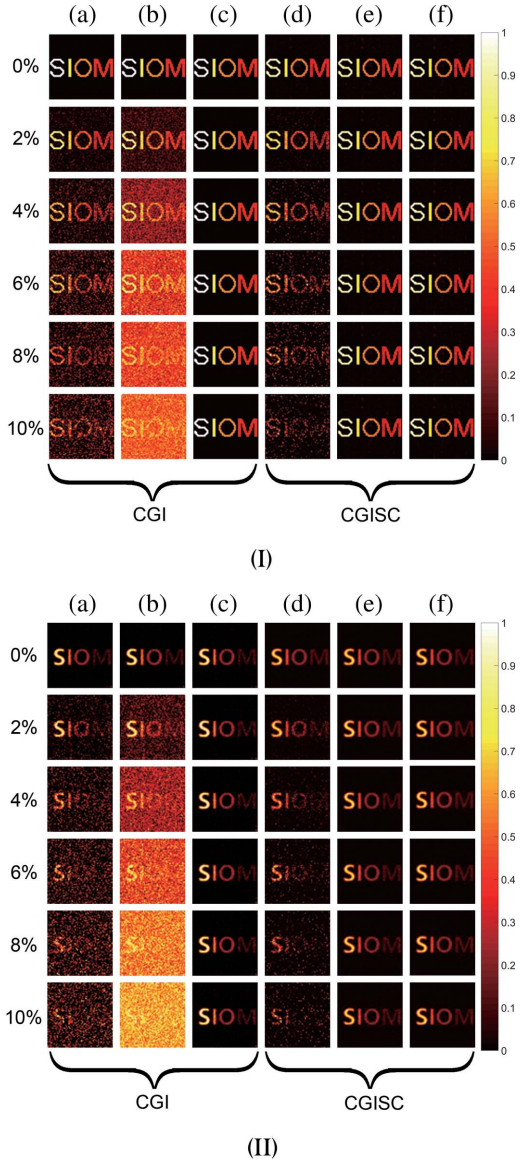

Fig. 3. Simulative and experimental results of imaging a reflection gray object (four letters "SIOM") when the RMS of the laser's energy fluctuation is 0%, 2%, 4%, 6%, 8%, and 10%, respectively. (I) Simulative results and (II) experimental results. (a) CGI with No Correction, (b) CGI with A Correction, (c) CGI with Y Correction, (d) CGISC with No Correction, (e) CGISC with A Correction, and (f) CGISC with Y Correction.

in different energy fluctuations. We can find that $\mathbf{M_C}$ is an identity matrix when the laser's energy is stable. As the RMS of the laser's energy fluctuation is increased, $\mathbf{M_C}$ will gradually deviate from the scalar matrix, which leads to the degradation of CGI. In addition, because the data of Y for the CGI system is usually small in practical applications, the method of Y Correction is of priority for both CGI and CGISC.

Finally, we apply the Y Correction method to our existing CGI lidar system (which is based on the principle structure of Fig. 2) to further demonstrate its feasibility. Figure 6(a) has given the statistical histogram of the pulsed laser's peak energy. According to Eq. (4), the RMS

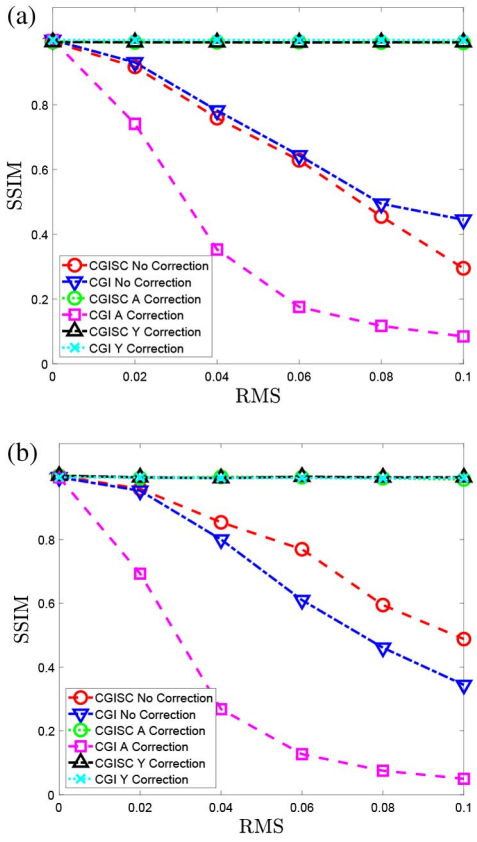

Fig. 4. Relationship between SSIM and RMS of the laser's energy fluctuation, based on the simulation and experimental results shown in Fig. 3. (a) The SSIM-RMS curves of the simulation results, and (b) the SSIM-RMS curves of the experimental results.

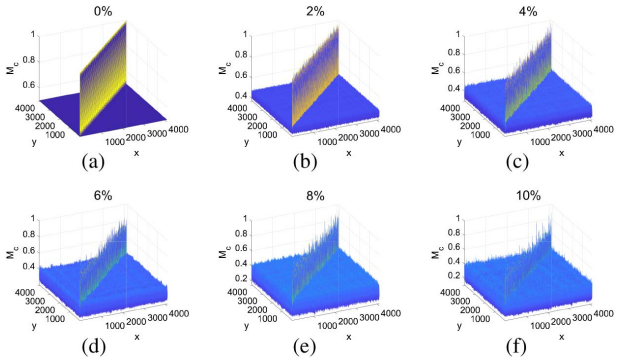

Fig. 5. $\mathbf{M}_C$ matrices for different energy fluctuations. The RMS of energy fluctuation of each matrix is 0% to 10% from (a) to (f).

value of the laser's energy fluctuation is 6.06%. Using the scene shown in Fig. 6(b) as the imaging target, the reconstruction results using CGI and CGISC with No Correction are displayed in Figs. 6(c) and 6(e), whereas Figs. 6(d) and 6(f) give the reconstruction results exploiting CGI and CGISC with Y Correction, respectively. It is clearly observed that the imaging quality can be obviously enhanced by the method of Y Correction, and is similar to

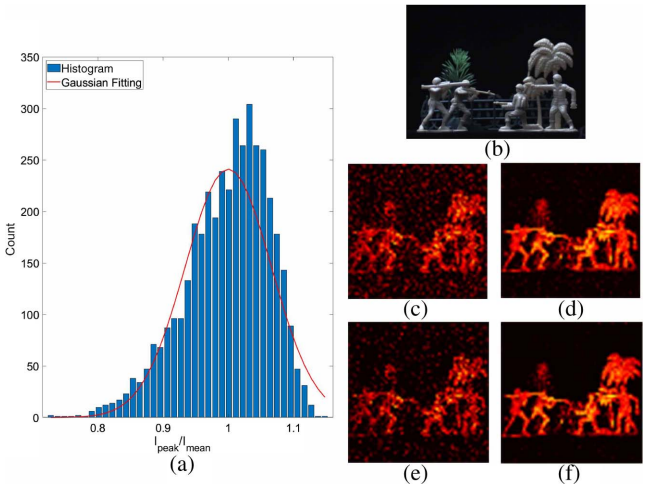

Fig. 6. Experimental demonstration result based on our existing CGI lidar system. (a) The histogram of the source's energy fluctuation and its corresponding Gaussian fitting, (b) the target, (c) and (e) are the reconstruction results of CGI and CGISC with No Correction, and (d) and (f) are the corresponding reconstruction results of CGI and CGISC with Y Correction.

the simulated and experimental results shown in Fig. 4 when the RMS of the laser's energy fluctuation is about 6%, which also suggests importance of the proposed approach in the applications of remote sensing.

In conclusion, the source's energy fluctuation will break the detection equation $\mathbf{Y} = \mathbf{AX}$, which CGI is mainly based on. We have demonstrated that the imaging quality of both CGI and CGISC is obviously degraded when $\mathbf{A}$ is a Hadamard coded matrix and the RMS of the source's energy fluctuation is greater than 2%. By monitoring the source's peak value of each pulse and dividing the echo signal by the corresponding peak value, the influence of the source's energy fluctuation on the reconstruction quality of both CGI and CGISC can be overcome. In addition, for CGISC, the method of A Correction with monitored peak value is also feasible, whereas invalid for CGI. This work is very helpful to CGI lidar in remote sensing where the energy fluctuation of the pulsed laser is usually large and CGI in the environment where the phenomenon of atmospheric scintillation is conspicuous.

This work was supported by the Youth Innovation Promotion Association of the Chinese Academy of Sciences, the Defense Industrial Technology Development Program of China (No. D040301), the National Natural Science Foundation of China (No. 61571427), and the Civil Aerospace Pre-research Project (No. D020214).

References

1. J. H. Shapiro, Phys. Rev. A **78**, 061802 (2008).
2. Y. Bromberg, O. Katz, and Y. Silberberg, Phys. Rev. A **79**, 053840 (2009).
3. X. Mei, W. Gong, Y. Yan, S. Han, and Q. Cao, Chin. J. Lasers **43**, 0710003 (2016).

4. Z.-H. Xu, W. Chen, J. Penuelas, M. Padgett, and M.-J. Sun, Opt. Express **26**, 2427 (2018).
5. X. Xu, E. Li, X. Shen, and S. Han, Chin. Opt. Lett. **13**, 071101 (2015).
6. H. Guo, R. He, C. Wei, Z. Lin, L. Wang, and S. Zhao, Chin. Opt. Lett. **17**, 071101 (2019).
7. O. Katz, Y. Bromberg, and Y. Silberberg, Appl. Phys. Lett. **95**, 131110 (2009).
8. C. Zhao, W. Gong, M. Chen, E. Li, H. Wang, W. Xu, and S. Han, Appl. Phys. Lett. **101**, 141123 (2012).
9. P. Clemente, V. Durán, E. Tajahuerce, and J. Lancis, Opt. Lett. **35**, 2391 (2010).
10. W. Gong and S. Han, Opt. Lett. **36**, 394 (2011).
11. M. Bina, D. Magatti, M. Molteni, A. Gatti, L. A. Lugiato, and F. Ferri, Phys. Rev. Lett. **110**, 083901 (2013).
12. W. Gong, C. Zhao, H. Yu, M. Chen, W. Xu, and S. Han, Sci. Rep. **6**, 26133 (2016).
13. M.-J. Sun, M. P. Edgar, G. M. Gibson, B. Sun, N. Radwell, R. Lamb, and M. J. Padgett, Nat. Commun. **7**, 12010 (2016).
14. C. Wang, X. Mei, L. Pan, P. Wang, W. Li, X. Gao, Z. Bo, M. Chen, W. Gong, and S. Han, Remote Sens. **10**, 732 (2018).
15. C. Wang, W. Gong, X. Shao, and S. Han, J. Opt. **18**, 065703 (2016).
16. K. Shibuya, K. Nakae, Y. Mizutani, and T. Iwata, Opt. Rev. **22**, 897 (2015).
17. M.-J. Sun, L.-T. Meng, M. P. Edgar, M. J. Padgett, and N. Radwell, Sci. Rep. **7**, 3464 (2017).
18. C. Zhou, T. Tian, C. Gao, W. Gong, and L. Song, J. Opt. **21**, 055702 (2019).
19. W. Gong, Photonics Res. **3**, 234 (2015).
20. G. H. Van Tartwijk and G. P. Agrawal, Prog. Quantum Electron. **22**, 43 (1998).
21. Z. Wang, E. P. Simoncelli, and A. C. Bovik, in *Thirty-Seventh Asilomar Conference on Signals, Systems & Computers* (2003), p. 1398.